ChemComm

COMMUNICATION

View Article Online
View Journal | View Issue

Cite this: *Chem. Commun.*, 2026, **62**, 5271

Received 8th December 2025,
Accepted 9th February 2026

DOI: 10.1039/d5cc06995e

rsc.li/chemcomm

One spiro to shift them all: tuning fluorescent organic nanoparticles emission *via* steric design

Eléonore Kurek, †[a] Ophélie Dal Pra, †[a] Aliocha Skrzypczak, ‡[a] Stéphane Massip, [b] Jonathan Daniel, [a] Mireille Blanchard-Desce *[a] and Chloé Grazon *[a]

Three quadrupolar fluorene-based dyes differing only by non-conjugated substituents form fluorescent organic nanoparticles (*d*FONs) with tunable emission from blue to yellow. A spirocyclic central substituent induces a marked red-shift *via* altered packing. When internalized into cells, *d*FONs evolve showing a characteristic blue-shift, enabling fluorescence-based monitoring of nanoparticle integrity and bioimaging performance.

Bioimaging applications require probes that not only emit brightly but also report on their physical and chemical state in complex environments. Conventional fluorescent nanoparticles (NPs) – whether inorganic quantum dots or dye-doped polymer/silica NPs – are designed for stability.[1,2] However, in the case of NPs based on supramolecular organization, such as micelles or aggregates, assessing if their structural integrity is retained within cells is trickier. Monitoring such nanoparticle disassembly usually requires multi-dye strategies or labelling approaches, which complicate synthesis and interpretation.[3–6]

Fluorescent organic nanoparticles (FONs), and in particular dye-based FONs (*d*FONs) obtained by nanoprecipitation of dedicated π-conjugated dyes, provide a promising alternative.[7,8] The spectral properties of *d*FONs are highly sensitive to the packing of the dye building blocks. Moreover, the fluorescence emission of *d*FONs made from polar and polarizable dyes is inherently sensitive to changes in the local environment, and supramolecular organization.[9] This makes *d*FONs ideal candidates for developing self-reporting nanoprobes whose spectral response directly reflects their aggregation state.

Here, we report a family of quadrupolar dyes differing only in their non-conjugated substituents on a fluorene core, which form self-stabilized organic nanoparticles with distinct packing geometries and emission colours. The resulting *d*FONs display strong structure-dependent spectral signatures – from blue to yellow emission – originating from different degrees of excitonic coupling features. When internalized by eukaryotic cells, the *d*FONs with strong excitonic coupling undergo a characteristic blue-shift in their emission, indicating a change in packing and environment of the constituting dyes. This demonstrates that fluorescence can serve as a direct optical readout of nanoparticle integrity, without requiring additional labelling or ratiometric design.

Three original quadrupolar dyes *dye·nC*$_9$, *dye·nC*$_4$ and *dye·spiC*$_4$ (Fig. 1a) with identical π-conjugated systems were synthesized through a three- or four step synthesis. They possess a common conjugated part, constituting an electron-donating fluorene core, flanked by two thienyl moieties conjugated with two electron-withdrawing amide end-groups. The dyes differ only in the nature of the alkyl pending substituents in the fluorene core, with *dye·nC*$_9$ bearing two nonyl chains, *dye·nC*$_4$ two butyl chains and *dye·spiC*$_4$ a spiro cycle (resulting in a spirofluorene core). The dyes are synthesized *via* a Pd-catalyzed Suzuki–Miyaura cross-coupling[10–12] between home-made 2,7-diiodospiro[alkyl-9,9-fluorene] (Scheme S1) and commercially available 5-carboxythiophene-2-boronic acid pinacol ester to introduce a conjugated carboxylic acid function (Scheme S2). The di-acid is then activated (Scheme S3) and reacted with benzylamine (Schemes S4 and S5) to yield the purified desired dyes with overall yields of 12%, 9% and 29% respectively for *dye·nC*$_9$, *dye·nC*$_4$ and *dye·spiC*$_4$ (^{1}H and ^{13}C NMR spectra provided in Fig. S2–S4).

The photophysical properties of the three dyes *dye·nC*$_9$, *dye·nC*$_4$ and *dye·spiC*$_4$ were first examined in THF (Table 1 and Table S2). Considering their identical conjugated systems, all three dyes share similar properties in solution; an absorption band peaking at 373 nm associated with a molar absorption coefficient ε^{max} at *ca.* 68 × 10^3 M^{-1} cm^{-1} and a fluorescence emission maximum of *ca.* 408 nm, associated with a fluorescence quantum yield Φ_F of *ca.* 0.70 and a fluorescence lifetime τ of 0.9 ns. The ε-normalized absorption spectra and normalized emission spectra of the dyes in THF are represented in grey in Fig. 1c and the solvatochromism of the dyes is depicted in Fig. S5: the three dyes exhibit no dependence of the absorption and emission spectra on solvent polarity, while the well-defined vibronic structures of the emission spectra indicates low

[a] *Univ. Bordeaux, CNRS, Bordeaux INP, ISM, UMR 5255, F-33400 Talence, France. E-mail: chloe.grazon@u-bordeaux.fr, mireille.blanchard-desce@u-bordeaux.fr*
[b] *Univ. Bordeaux, CNRS, INSERM, IECB, UAR 3033, F-33600 Pessac, France*
† These authors contributed equally to this work.
‡ Present address: Univ Rennes, INSA Rennes, CNRS, ISCR (Institut des Sciences Chimiques de Rennes), UMR 6226, Université de Rennes, Rennes, France.

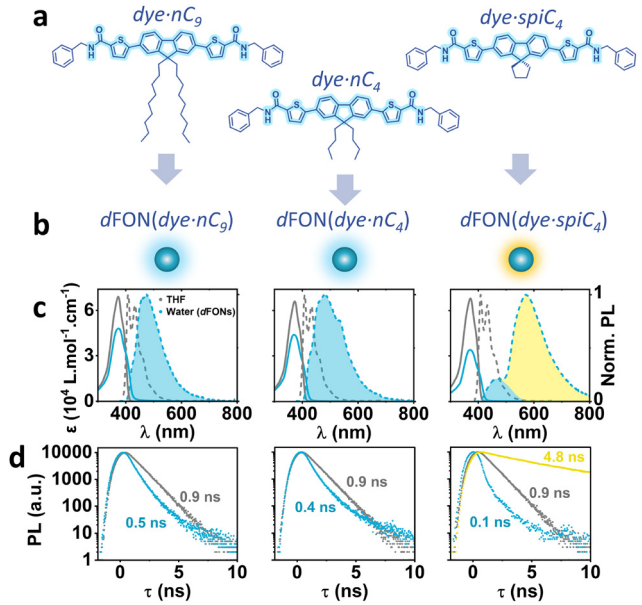

Fig. 1 (a) Molecular structures of blue-emitting fluorophores *dye·nC*$_9$, *dye·nC*$_4$ and *dye·spiC*$_4$. The grey arrows symbolize the preparation of *d*FONs from the dyes through nanoprecipitation in water (Fig. S1). (b) Schematic representation of *d*FONs and their emission colour. (c) Molar absorption coefficient (full lines) and normalized emission spectra upon excitation at 370 nm (dashed lines) of *dye·nC*$_9$, *dye·nC*$_4$, and *dye·spiC*$_4$ in THF (grey) and of *d*FON(*dye·nC*$_9$), *d*FON(*dye·nC*$_4$), and *d*FON(*dye·spiC*$_4$) in water (blue). (d) Fluorescence decays upon excitation at 370 nm of *dye·nC*$_9$, *dye·nC*$_4$ and *dye·spiC*$_4$ in THF (grey) and of *d*FON(*dye·nC*$_9$), *d*FON(*dye·nC*$_4$) and *d*FON(*dye·spiC*$_4$) in water (blue) at 450 nm or at 590 nm (yellow), measured using time-correlated single photon counting. Fitted fluorescence lifetimes in caption.

interaction of the excited state with the solvent. This indicates that no symmetry-breaking occurs in the excited state.

The three *d*FONs were prepared from these three dyes using the nanoprecipitation method (Fig. S1): a 0.5 mM stock solution of dye in THF : DMSO (9 : 1) was added dropwise to a large volume of distilled water under magnetic stirring, such that the final proportion of organic solvent did not surpass 1%. This process yielded colourless and non-turbid colloidal dispersions of *d*FONs.

The photophysical properties of the resulting nanoparticles *d*FON(*dye·nC*$_9$), *d*FON(*dye·nC*$_4$) and *d*FON(*dye·spiC*$_4$) were then investigated (Table 1 and Table S2). The normalized absorption and emission spectra of the *d*FONs are represented in blue in Fig. 1c (full normalized spectra in Fig. S5). While the absorption spectra of *d*FON(*dye·nC*$_9$) and *d*FON(*dye·nC*$_4$) are quite similar to their molecular counterparts in THF, *d*FON(*dye·spiC*$_4$) presents a 10 nm hypsochromic shift. Additionally, the molecular ε of dyes as building blocks of *d*FON(*dye·nC*$_9$) and *d*FON(*dye·nC*$_4$) was *ca.* 30% lower than that of the dyes in THF, while that for *d*FON(*dye·spiC*$_4$) was 50% lower. This hypochromic effect, along with the slight broadening (Fig. 1c and Fig. S5) of the absorption band were reported before in closely related systems[9,12] and were attributed to excitonic splitting.[15,16] The most striking differences by far are found in the *d*FONs emissive properties. Compared to the molecular dyes in solution, all *d*FONs display a broadened and bathochromically shifted emission, with a loss of vibronic structure (Fig. 1c and Table 1). *d*FON(*dye·nC*$_9$) and *d*FON(*dye·nC*$_4$) emission spectra are not identical but close, with an emission at 475 nm and 481 nm, respectively. The spectral shape of *d*FON(*dye·nC*$_4$) is slightly broader and displays a small additional shoulder around 540 nm. These observed changes in the shape, position, and intensity of the emission spectrum are a common occurrence in *d*FONs, due to intermolecular interactions. In addition, the fluorescence quantum yields (Φ_F) of *d*FON(*dye·nC*$_9$) (Φ_F = 0.23) and *d*FON(*dye·nC*$_4$) (Φ_F = 0.15) are lower than that of the dyes in THF solutions. This trend arises from two key factors: a slight reduction in the radiative rate constant (k_r) in relation to the interchromophoric interactions within the aggregated *d*FONs, and a marked increase in the non-radiative rate constant (k_{nr}) (Table 1 and Fig. S6), which might be ascribed to vibrational deactivation due to water molecules in close proximity to the surface of the nanoparticle.[17] We also stress that the fluorescence emission of crystals of *dye·nC*$_9$ and *dye·nC*$_4$ does not overlap with the corresponding *d*FONs spectra (Fig. S8), suggesting the amorphous nature of these molecular aggregates.

In comparison, *d*FON(*dye·spiC*$_4$) emissive properties are strikingly different: the spectrum comprises a main band at 569 nm, and a minor band (about 15% of the main band in height) at 466 nm, resembling that of *d*FON(*dye·nC*$_9$) and *d*FON(*dye·nC*$_4$). Concomitantly, the fluorescence quantum yield is drastically reduced, down to 0.03, and the fluorescence lifetime is significantly increased to 4.8 ns at 590 nm (Fig. 1d and Fig. S6, S7). We attribute this new band in the yellow region to strong excitonic coupling,[16,18] which stabilizes a low-energy emissive state, thus reducing k_r and enhancing k_{nr} and resulting in reduced brightness. The fact that only *d*FON(*dye·spiC*$_4$) exhibit this band indicates that the rigid nature of the spiro

Table 1 Photophysical and structural properties of the three dyes in THF and of the associated *d*FONs in water, at 20 °C

Sample	Solvent	λ_{abs}^{max} [a] (nm)	ε^{max} [b] ($\times 10^3$ M^{-1} cm^{-1})	$\Delta\nu$ [c] (cm^{-1})	λ_{em}^{max} [d] (nm)	Φ_F [e]	τ_{amp} [f] (ns)	k_r [g] (ns^{-1})	k_{nr} [h] (ns^{-1})	B_V [i] ($\times 10^3$ M^{-1} cm^{-1} nm^{-3})
dye·nC$_9$	THF	373	69 ± 8	2300	408	0.72 ± 0.02	0.9	0.8	0.3	35
*d*FON(*dye·nC*$_9$)	H_2O	374	48 ± 8	5685	475	0.23 ± 0.01	0.5	0.5	1.5	8
dye·nC$_4$	THF	373	66 ± 2	2360	409	0.65 ± 0.03	0.9	0.7	0.4	36
*d*FON(*dye·nC*$_4$)	H_2O	370	44 ± 2	6237	481	0.15 ± 0.01	0.4	0.4	2.1	6
dye·spiC$_4$	THF	372	68 ± 2	2372	408	0.70 ± 0.03	0.9	0.8	0.3	44
*d*FON(*dye·spiC*$_4$)	H_2O	362	34 ± 2	10 050	569 (466)	0.03 ± 0.01	0.1/4.8*	0.1/0.01*	10/0.2*	0.9

A more comprehensive version of this table is provided in the SI (Table S1).[a] Absorption maximum wavelength. [b] Molar absorption coefficient of the dyes at λ_{abs}^{max} (in solution in THF or as *d*FONs subunits), measured from three differently prepared solutions and subsequent dilutions (error bars correspond to the standard deviation on all points). [c] Stokes shift. [d] Emission maximum wavelength. [e] Relative fluorescence quantum yield. [f] Amplitude-averaged fluorescence lifetime, using λ_{exc} = 370 nm and λ_{em} = 450 nm, except for (*): λ_{em} = 590 nm. [g] Radiative rate constant. [h] Non-radiative rate constant. [i] Brightness per volume. All steady-state fluorescence emission spectra were recorded using λ_{exc} = 370 nm.

substituent and its small size play a crucial role, by strongly affecting molecular packing within *d*FONs. This showcases the importance of the nature of the substituents in dye design for *d*FONs.[9,19]

For comparison, a dye bearing the same spiro substituent but with benzyl-amide groups replaced by diethyl-imide groups (*dye·spiC*$_4$ *NEt*$_2$ (6), Scheme S6, Fig. S5–S7 and Tables S1, S2)[12] exhibits only a weak red shoulder in its emission. In addition, the crystal structures of *dye·spiC*$_4$ and *dye·spiC*$_9$ (Fig. S11, S12 and Tables S3, S4) indicate that the benzyl-amide groups could play a role in the molecular arrangement of the dyes. This suggests that, beyond the spiro unit promoting closer dye proximity compared to extended alkyl chains, the benzyl-amide groups at the dye termini may also modulate the spatial organization of the dyes within dFONs, thereby influencing their optical properties. The effective Stokes Shift of *d*FON(*dye·spiC*$_4$) is huge compared to that of *d*FON(*dye·nC*$_9$) and *d*FON(*dye·nC*$_4$) (10×10^3 cm^{-1} compared to 6×10^3 cm^{-1}).

The morphological characteristics of *d*FONs were investigated using transmission electron microscopy (TEM), as illustrated in Fig. 2 and Fig. S9. *d*FON(*dye·nC*$_9$) and *d*FON(*dye·nC*$_4$) appeared as spherical nanoparticles with mean diameters of 35–40 nm. *d*FON(*dye·spiC*$_4$) were found to exhibit polymorphism, with one population of spherical nanoparticles, averaging *ca.* 35 nm in diameter and a second population of "rod-like" particles, measuring roughly 20 nm in width and from 20 up to 150 nm in length.

The average number of dyes per nanoparticles (N, eqn (S1)) is derived from the *d*FONs dry diameter. The theoretical brightness (B, eqn (S4), Table S1 and Fig. S10) and brightness per volume (B_V, eqn (S5), Table 1) of the NPs are then calculated. While *d*FON(*dye·nC*$_9$) and *d*FON(*dye·nC*$_4$) have a similar brightness around 2×10^8 M^{-1} cm^{-1}, the brightness of *d*FON(*dye·spiC*$_4$) is ten times lower (2×10^7 M^{-1} cm^{-1}). This resulted in brightnesses per volume around 7×10^3 M^{-1} cm^{-1} nm^{-3} for *d*FON(*dye·nC*$_9$) and *d*FON(*dye·nC*$_4$) and 0.9×10^3 M^{-1} cm^{-1} nm^{-3} for *d*FON(*dye·spiC*$_4$). The B_V of *d*FONs containing dyes with alkyl chains is approximately ten times higher than that of PMMA nanoparticles doped with blue-emitting cyanine ($B_V = 7 \times 10^2$ M^{-1} cm^{-1} nm^{-3}) for NPs of comparable size.[20] In contrast, *d*FON(*dye·spiC*$_4$) exhibit a 100-fold higher overall brightness compared to QD540 ($B = 1.7 \times 10^5$ M^{-1} cm^{-1}),[21] while showing a similar brightness per unit volume ($B_{V,QD540} = 1.5 \times 10^3$ M^{-1} cm^{-1} nm^{-3}), which can be attributed to the smaller size of bare QDs.

Finally, before using these nanoparticles in biological applications, their colloidal stabilities in different media (water or cell culture medium) were evaluated (Fig. S13). Over 24 hours, neither a change in absorbance nor setting was observed. This confirms the good colloidal stability of the *d*FONs in such conditions and supports their potential use in cell culture medium. In addition, the emissive properties of the *d*FON(*dye·spiC*$_4$) were evaluated in supplemented cell culture media (DMEM + FBS) (Fig. S14). Overall the emissive spectra remain the same, but a decrease of the band at 570 nm and an increase of the band at 466 nm is observed.

*d*FON(*dye·spiC*$_4$) were then evaluated as bioimaging probes in fluorescence microscopy experiments on HEK and COS-7 cells (Fig. 3 and Fig. S15, S16). First, the *d*FONs were incubated with HEK cells in DMEM supplemented with 10% FBS. Live, wash-free imaging was then conducted over one hour to monitor the intracellular fate of the nanoparticles. Under these conditions,

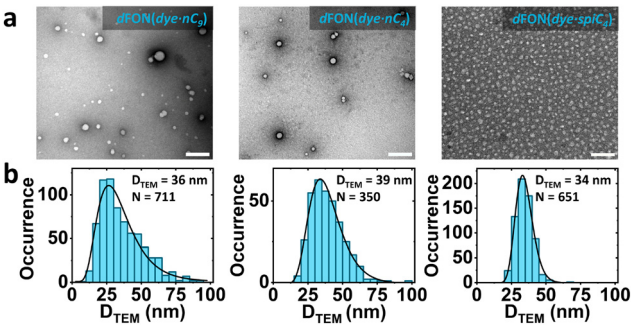

Fig. 2 (a) Transmission electron microscopy images of *d*FON(*dye·nC*$_9$), *d*FON(*dye·nC*$_4$) and *d*FON(*dye·spiC*$_4$), negatively stained using uranyl acetate. Scale bar: 200 nm; (b) size distribution of *d*FONs dry diameters measured from TEM images. Caption: resulting mean dry diameters of dFONs (D_{TEM}) and number of measured particles (N). Note that for *d*FONs(*dye·spiC*$_4$), only spherical nanoparticles were counted for the size distribution.

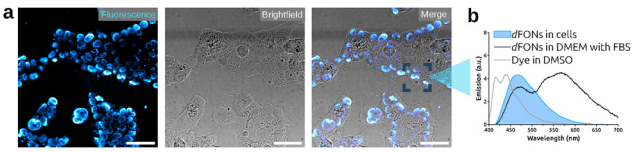

Fig. 3 (a) Fluorescence microscopy images of *d*FON(*dye·spiC*$_4$) at 5 nM in live HEK cells in DMEM + 10%FBS cell-culture medium (incubation time = 54 min.). Scale bar: 50 μm. λ_{exc} = 405 nm, λ_{em} = 415–500 nm. (b) Raw *in cellulo* emission spectra of *d*FON(*dye·spiC*$_4$) within the cells (blue), overlayed on the corresponding normalized emission spectra of dFONs in DMEM with FBS (10%, black) and of the dye in solution in dimethylsulfoxide (DMSO, grey).

only the *d*FONs that had entered or were concentrated inside the cells could be detected, whereas dispersed nanoparticles in the culture medium remained below the detection threshold.

After approximately one hour, the *d*FONs accumulated inside the cells and displayed an emission band with a maximum around 460 nm (Fig. 3). This emission does not overlap with that of the *d*FONs in DMEM + FBS, nor with that of the isolated *dye·spiC*$_4$ in a polar solvent such as DMSO. Instead, it closely resembles the emission of *d*FON(*dye·nC*$_4$) or *d*FON(*dye·nC*$_9$). To further investigate this unexpected behaviour, the intracellular accumulation of *d*FON(*dye·spiC*$_4$) was monitored at *ca.* 30, 40, 50 and 90 min (Fig. S15). Remarkably, the nanoparticles entered the cells rapidly, within *ca.* 30 min, and continued to accumulate over the full duration of the experiment. Concomitantly, the fluorescence emission of *d*FON(*dye·spiC*$_4$) underwent a pronounced hypsochromic shift.

We hypothesize that upon cell internalization, the *d*FONs undergo a structural reorganization within the cellular environment while remaining in an aggregate state. Such a reorganization would account for the loss of excitonic coupling signatures, while maintaining an emission profile characteristic of aggregated dyes rather than isolated chromophores.

To assess whether this behavior was cell-line dependent, we also incubated *d*FON(*dye·spiC*$_4$) with COS-7 cells and imaged them after 2 h (Fig. S16). Strikingly, the fluorescence signal was again centered around 450 nm and the excitonic coupling signature was lost. These observations indicate that the *d*FONs exhibit the same intracellular

behavior regardless of the cell line investigated (fibroblast or embryonic).

Our study demonstrates that a single substituent modification on a dye can drastically alter its solid-state properties, leading in our case to a pronounced red-shift in emission. This unique spectral signature provides an efficient means to monitor the aggregation state of fluorophores within nanoparticles without the need for mixed-dye systems – an important asset for applications such as biosensing or drug-delivery, where controlling nanoparticle behaviour is essential. In living cells, *d*FON(*dye*·*spiC*$_4$) displays a markedly broadened and blue-shifted emission compared to *d*FONs in aqueous suspension, a behaviour that indicates a loss of excitonic coupling promoted either by the dissociation of the nanoaggregates (as previously observed for other *d*FONs[3]) or by reorganization of the dyes within the assemblies. What makes this system truly innovative is its reliance on a single dye component, which—despite its simplicity—achieves dramatic fluorescence signal modulation in cells. This modulation is driven entirely by the dynamic reorganization of the dyes within the nanoparticle, rather than the conventional "off/on" mechanisms seen in most systems (where fluorescence is quenched in aggregated states and only recovers upon nanoparticle dissolution in biological media)[22] or solvatochromic effects, where the dissolution of the nanoparticles is followed by a change in the fluorescence signal.[23] Importantly, the optical tuning is achieved here while preserving the nanoparticle features associated with high brightness. Such sensitivity to the cellular environment, combined with distinct staining profiles across cell lines, highlights that the nature of the dye substituents has a strong influence on the cellular fate of *d*FONs (as already demonstrated for other systems[9,24]) and further supports their potential for controlled sensing[12] and drug-delivery applications.[25]

CRediT: Eleonore Kurek: investigation, validation, methodology, visualisation, writing – original draft preparation. Ophélie Dal Pra: investigation, visualisation, writing – review & editing. Aliocha Skrzypczak: investigation, writing – Review & Editing. Stéphane Massip: investigation, data curration. Jonathan Daniel: investigation, visualization, writing – review & editing. Mireille Blanchard-Desce: conceptualization, funding acquisition, supervision, writing – review & editing. Chloé Grazon: conceptualization, data curation, funding acquisition, methodology, project administration, supervision, visualisation, writing – original draft preparation.

Conflicts of interest

There are no conflicts to declare.

Data availability

Data for this article are available at Zenodo repository 18324973.

Supplementary information (SI): materials and methods, chemical characterizations of dyes, extra photophysical datas, bioimaging. See DOI: https://doi.org/10.1039/d5cc06995e.

CCDC 2524470 and 2524471 contain the supplementary crystallographic data for this paper.[26a,b]

Acknowledgements

The synthesis of dyes 5b and 6 were performed by J. Traisnel and A. Okba, respectively. This project has received funding from the European Research Council (ERC) under the European Union's Horizon Europe research and innovation program (Grant agreement no. 101077364). Financial support for ODP and EK was provided through the MENESR (Ministère de l'Education Nationale, de l'Enseignement Supérieur et de la Recherche) of France. This work has also benefited from the LIGHT S&T Graduate Program (PIA 3 Investment for Future Program, ANR-17-EURE-0027), support and facilities and expertise of IECB Biophysical and Structural Chemistry platform (BPCS), CNRS UAR3033, Inserm US001, Univ Bordeaux. Continuous support from the University of Bordeaux, Bordeaux-INP and CNRS is greatly acknowledged.

References

1 W. R. Algar, A. Szwarczewski and M. Massey, *Anal. Chem.*, 2023, **95**, 551–559.
2 W. R. Algar, M. Massey, K. Rees, R. Higgins, K. D. Krause, G. H. Darwish, W. J. Peveler, Z. Xiao, H.-Y. Tsai, R. Gupta, K. Lix, M. V. Tran and H. Kim, *Chem. Rev.*, 2021, **121**, 9243–9358.
3 J. Boucard, T. Briolay, T. Blondy, M. Boujtita, S. Nedellec, P. Hulin, M. Grégoire, C. Blanquart and E. Ishow, *ACS Appl. Mater. Interfaces*, 2019, **11**, 32808–32814.
4 N. Curtin, M. Garre, J.-B. Bodin, N. Solem, R. Méallet-Renault and D. F. O'Shea, *RSC Adv.*, 2022, **12**, 35655–35665.
5 M. Zhang, C. Wang, C. Yang, H. Wu, H. Xu and G. Liang, *Anal. Chem.*, 2021, **93**, 5665–5669.
6 S. W. Morton, X. Zhao, M. A. Quadir and P. T. Hammond, *Biomaterials*, 2014, **35**, 3489–3496.
7 V. Parthasarathy, S. Fery-Forgues, E. Campioli, G. Recher, F. Terenziani and M. Blanchard-Desce, *Small*, 2011, **7**, 3219–3229.
8 S. Fery-Forgues, *Nanoscale*, 2013, **5**, 8428–8442.
9 J. Daniel, O. D. Pra, E. Kurek, C. Grazon and M. Blanchard-Desce, *C. R. Chim*, 2024, **27**, 1–17.
10 J. Daniel, A. G. Godin, M. Palayret, B. Lounis, L. Cognet and M. Blanchard-Desce, *J. Phys. D: Appl. Phys.*, 2016, **49**, 084002.
11 H. Li, J. Daniel, J.-B. Verlhac, M. Blanchard-Desce and N. Sojic, *Chem. – Eur. J.*, 2016, **22**, 12702–12714.
12 O. Dal Pra, J. Daniel, G. Recher, M. Blanchard-Desce and C. Grazon, *Small Methods*, 2024, **8**, 2400716.
13 D. F. Eaton, *Pure Appl. Chem.*, 1988, **60**, 1107–1114.
14 K. Rurack and M. Spieles, *Anal. Chem.*, 2011, **83**, 1232–1242.
15 M. Kasha, H. R. Rawls and M. Ashraf El-Bayoumi, *Pure Appl. Chem.*, 1965, **11**, 371–392.
16 A. S. Davydov, *Phys.-Usp.*, 1964, **7**, 145.
17 J. Maillard, K. Klehs, C. Rumble, E. Vauthey, M. Heilemann and A. Fürstenberg, *Chem. Sci.*, 2021, **12**, 1352–1362.
18 J. Gierschner, J. Shi, B. Milián-Medina, D. Roca-Sanjuán, S. Varghese and S. Park, *Adv. Opt. Mater.*, 2021, **9**, 2002251.
19 J. Daniel, *These de doctorat*, Bordeaux, 2015.
20 P. Ashokkumar, N. Adarsh and A. S. Klymchenko, *Small*, 2020, **16**, 2002494.
21 R. Gupta, W. J. Peveler, K. Lix and W. R. Algar, *Anal. Chem.*, 2019, **91**, 10955–10960.
22 J. Boucard, C. Linot, T. Blondy, S. Nedellec, P. Hulin, C. Blanquart, L. Lartigue and E. Ishow, *Small*, 2018, **14**, 1802307.
23 A. Faucon, H. Benhelli-Mokrani, L. A. Córdova, B. Brulin, D. Heymann, P. Hulin, S. Nedellec and E. Ishow, *Adv. Healthcare Mater.*, 2015, **4**, 2727–2734.
24 A. H. A. M. V. Onzen, L. Albertazzi, A. P. H. J. Schenning, L.-G. Milroy and L. Brunsveld, *Chem. Commun.*, 2017, **53**, 1626–1629.
25 A. Jana, K. S. P. Devi, T. K. Maiti and N. D. P. Singh, *J. Am. Chem. Soc.*, 2012, **134**, 7656–7659.
26 (*a*) CCDC 2524470: Experimental Crystal Structure Determination, 2026, DOI: 10.5517/ccdc.csd.cc2qqxjx; (*b*) CCDC 2524471: Experimental Crystal Structure Determination, 2026, DOI: 10.5517/ccdc.csd.cc2qqxky.

